RMetS
Royal Meteorological Society

# Aerosol indirect effects on glaciated clouds. Part I: Model description

Innocent Kudzotsa,[a]* Vaughan T. J. Phillips,[b] Steven Dobbie,[c] Marco Formenton,[b] Jiming Sun,[d] Grant Allen,[e] Aaron Bansemer,[f†] Dominick Spracklen[c] and Kirsty Pringle[c]

[a]*Department of Physics, University of Zimbabwe, Harare, Zimbabwe*
[b]*Department of Physical Geography and Ecosystem Science, University of Lund, Sweden*
[c]*School of Earth and Environment, University of Leeds, UK*
[d]*Institute of Atmospheric Physics, Chinese Academy of Science, Beijing, China*
[e]*School of Earth, Atmospheric and Environmental Sciences, University of Manchester, UK*
[f]*National Center for Atmospheric Research, Boulder, Colorado, USA*

*Correspondence to: I. Kudzotsa, Department of Physics, University of Zimbabwe, MP 167 Mt Pleasant, Harare, Zimbabwe. E-mail: ikudzotsa@gmail.com
[†]This article has contributions by a US Government employee and his work is in the public domain in the USA

**Various improvements were made to a state-of-the-art aerosol–cloud model and comparison of the model results with observations from field campaigns was performed. The strength of this aerosol–cloud model is in its ability to explicitly resolve all the known modes of heterogeneous cloud droplet activation and ice crystal nucleation. The model links cloud particle activation with the aerosol loading and chemistry of seven different aerosol species. These improvements to the model resulted in more accurate prediction especially of droplet and ice crystal number concentrations in the upper troposphere and enabled the model to directly sift the aerosol indirect effects based on the chemistry and concentration of the aerosols. In addition, continental and maritime cases were simulated for the purpose of validating the aerosol–cloud model and for investigating the critical microphysical and dynamical mechanisms of aerosol indirect effects from anthropogenic solute and solid aerosols, focusing mainly on glaciated clouds. The simulations showed that increased solute aerosols reduced cloud particle sizes by about 5 μm and inhibited warm rain processes. Cloud fractions and their optical thicknesses were increased quite substantially in both cases. Although liquid mixing ratios were boosted, there was however a substantial reduction of ice mixing ratios in the upper troposphere owing to the increase in snow production aloft. These results are detailed in the subsequent parts of this study.**

*Key Words:* aerosol-cloud interactions; cloud microphysics; cloud-resolving models; aerosols; aerosol indirect effects

*Received 21 August 2015; Revised 8 March 2016; Accepted 11 March 2016; Published online in Wiley Online Library 26 April 2016*

## 1. Introduction

According to the Intergovernmental Panel on Climate Change (IPCC) reports (Solomon *et al.*, 2007; Boucher *et al.*, 2013), aerosols are one of the major climate forcing agents, and they do so in two major pathways. Firstly, by directly interacting with solar radiation (Charlson *et al.*, 1992; Liao and Seinfeld, 1998; Myhre *et al.*, 2009) and indirectly by altering the optical or radiative properties of clouds (Charlson *et al.*, 1992; Haywood and Boucher, 2000; Lohmann and Feichter, 2005; O'Donnell *et al.*, 2011; Gettelman *et al.*, 2012). The latter pathway is referred to as the *aerosol indirect effect* (AIE) and is the subject of this article. There is also the *semi-direct* effect, which is caused by absorbing aerosols (Lohmann and Feichter, 2001; Johnson *et al.*, 2004). These absorbing aerosols have a heating effect in the atmosphere, which may subsequently cause the evaporation of cloud particles (Johnson, 2003; Hill and Dobbie, 2008; Koch and Genio, 2010).

In order to investigate the effects of the aerosols on a global scale, the use of General Circulation Models (GCMs) is required (Lohmann *et al.*, 2007). However, these AIEs are affected by subgrid-scale microphysical processes, which are too small to resolve in coarse resolution GCMs (McComiskey and Feingold, 2012). Therefore, to circumvent this challenge, aerosol–cloud microphysical processes have to be incorporated into GCMs by way of parametrizations (Menon *et al.*, 2002a; Lohmann and Feichter, 2005; Gettelman *et al.*, 2012). These parametrizations are developed from the use of higher-resolution models, such as the Cloud System Resolving Models (CSRMs) (Phillips *et al.*, 2009; Morrison and Grabowski, 2011).

In order to rigorously investigate and evaluate the most critical effects of aerosols on radiation via the clouds by numerical techniques, it is essential that the numerical model being used is able to resolve the relevant microphysical and dynamical cloud processes at the temporal and spatial scales that are pertinent to

real clouds. Hence, the version of the numerical model used in this study is an aerosol–cloud model coupled to the Weather Research and Forecasting (WRF) model. The previous version of this model is described by Phillips *et al.* (2007, 2009). It was a bulk-microphysics model, which included double-moment microphysics in cloud and a single moment in precipitation processes. The empirical parametrization for heterogeneous ice nucleation of Phillips *et al.* (2009) was already incorporated in that version of the model. In addition, the 2009 version of the model consisted of a semi-prognostic aerosol component responsible for the replenishment of environmental aerosols. This earlier version of the model was used to investigate the influence of increased aerosol on the microphysical properties of clouds. It was discovered that increased concentrations of primary biological aerosol particles (PBAPs) boosted the number concentrations of ice crystals by about 100% (mostly due to the intensification of both heterogeneous ice nucleation and homogeneous freezing of supercooled cloud droplets) and also at least doubled the cloud droplet concentrations mostly due to the cloud condensation nuclei (CCN) activity of extra insoluble organic particles. Also, the mean sizes of these particles were found to diminish as a result of increased competition for available vapour from extra cloud and ice particles. However, this previous version has since been transformed into a hybrid bin/bulk microphysics scheme, enabling the model to resolve essential aerosol–cloud interaction processes explicitly, while other ancillary processes were treated implicitly in order to reduce the model's computational expense.

Double-moment schemes have proved to be superior over single-moment schemes in terms of accuracy, especially in simulating precipitation in deep convective cells (Lim and Hong, 2010). Due to the prediction of extra terms in double-moment schemes, their computational expense is amplified, hence curtailing their use in real-time weather forecasting and climate prediction models; however, they provide a more accurate understanding especially of cloud and precipitation processes. This is the scope within which the double-moment bulk microphysics scheme presented here was developed.

The following modifications were applied to the aerosol–cloud model to improve its performance, particularly on the treatment of cloud processes that are crucial in addressing aerosol–cloud interactions. The sulphate aerosol group was dualised by splitting the two modes of sulphate aerosols (the fine and the accumulation modes) and treating them as two independent aerosol species. This development was meant to improve the treatment and budgeting of aerosols especially in the activation of cloud droplets and nucleation of ice crystals. In addition to this dualisation of the sulphate aerosol species, a two-moment treatment was also incorporated for the same aerosol group. This enables a more accurate prediction of their mean sizes (which are important in the nucleation process cloud droplets and cloud ice) rather than prescribing them *a priori*. This special treatment was coded only for sulphate aerosols because of their dominance in the atmosphere in terms of number concentrations and their superior influence as CCN over other aerosol species.

Emulated bin microphysics, or the explicit integration of microphysics processes, has also been implemented to all coagulation processes (e.g. riming, aggregation and accretion). This explicit microphysics of coagulation processes provides a more accurate approach for treating the interaction of cloud and precipitation particles with each other. This development ensures that cloud development, changes of cloud phases and precipitation production are rigorously resolved. This was not only a major improvement to the model, but also very relevant and necessary in the research of aerosol–cloud interactions. Following the introduction of the emulated bin microphysics approach to the coagulation processes, there was need to incorporate ice morphology into the model in order to allow accurate treatment of the collision and sticking efficiencies during particle interactions, taking into account their dependence on temperature and sizes.

A number of researchers (e.g. Clark, 1974; Mitchell and Arnott, 1994; Walko *et al.*, 1995) have shown that a gamma distribution is a more appropriate representation of the size distribution of hydrometeors. Hence, in this version of the model, a gamma distribution has been used for all precipitation hydrometeors replacing the old exponential one (Kessler, 1969), which was implemented in the previous versions of the model. A common approach of fixing the intercept parameters for the size distribution was avoided here by introducing either temperature- or mixing ratio-dependent intercept parameters of Reisner *et al.* (1998) and Thompson *et al.* (2004). This was done because a study by Reisner *et al.* (1998) showed that fixing the intercept parameters promoted excessive depletion of cloud water.

Since the introduction of an empirical parametrization of heterogeneous ice nucleation by Phillips *et al.* (2008), there has been advancement in the knowledge of the chemistry, composition and nucleating abilities of aerosols. Hence, Phillips *et al.* (2013) took the new available knowledge of ice nuclei and their nucleation abilities into consideration and modified his empirical parametrization. This modified version of the empirical parametrization of heterogeneous nucleation of cloud ice by Phillips *et al.* (2013) was also incorporated into this version of the model. The most interesting and relevant improvement here is that soluble organics are now allowed to nucleate ice crystals at appropriate temperatures and supersaturations in line with recent laboratory observations of Murray *et al.* (2010).

The structure of this article is as follows. In section 2, the aerosol–cloud model used in this study is described. The description of the cases simulated, set-up and validation of the model will be given in section 3. The discussion of the model performance and results are given in section 4. Finally, conclusions and future work will be stated in section 5.

## 2. Model description

### 2.1. Overview

The numerical model used here is an aerosol-cloud model coupled to the Weather Research and Forecasting (WRF) model. The original version of this model was described in Phillips *et al.* (2007, 2008, 2009); however, it has now been transformed into a hybrid bin/bulk microphysics scheme. Improvements to the heterogeneous ice nucleation scheme described in Phillips *et al.* (2013) have since been incorporated into this present microphysics scheme. This model is a CSRM, which has prognostic variables of a two-moment hybrid bin/bulk microphysics for all cloud liquid and precipitation species. The CSRM is a non-hydrostatic and an anelastic fluid flow model with periodic boundary conditions and forty vertical levels. In this study, the vertical resolution is approximately 500 m, with the model top set at 20 km. The model grids are 2 km wide, with the whole domain size being 170 km. The integration time step of 10 s is used. Prognostic microphysical variables are written out every 5 min for analysis.

For the cases simulated in this project, a two-dimensional domain is applied. Convection is maintained in a standard way by including additional tendencies of heat and moisture. The tendencies are specified from the derived large-scale forcing, observed from a network of soundings used in the respective cases simulated (section 3.1). These tendencies are added as extra sources to the evolution equations for potential temperature and vapour mixing ratio.

### 2.2. The microphysics scheme

#### 2.2.1. The aerosol treatment

The aerosol–cloud model has a semi-prognostic aerosol component (Phillips *et al.*, 2009) comprising a complement of seven different aerosol species. The insoluble organic aerosol group is split into primary biological aerosols (PBAPs), which may include pollen, bacteria, fungal spores, viruses, plant and

 

animal fragments and non-biological insoluble organics following (Phillips *et al.*, 2013). In addition, the larger and smaller modes of the sulphate aerosol group are prognosed independently and treated as two different aerosol species. Furthermore, a fraction of soluble organic aerosols now acts as IN at relevant temperatures (below −65 °C) and supersaturations according to Murray *et al.* (2010). This gives an aerosol complement of nine species, each with independent prognostic variables such as mass and number mixing ratios.

These aerosols are classified into two main categories, soluble and solid aerosols. The classification of the chemical composition of the aerosols follows that commonly found in some of the most modern GCMs.

- The soluble aerosol species are ammonium sulphate (its bi-modal distribution is separated into two independent modes as $SO4_1$ and $SO4_2$), sea-salt (SS) and soluble organic carbonaceous material (SO).
- The insoluble aerosol group comprises mineral dust/metallic (DM), soot/black carbon (BC), insoluble non-biological organic (O), primary biological aerosol particles (BIO) and finally there is a fraction of the soluble organic group (SO) that becomes glassy at very low temperatures (SOLO).

All species can nucleate liquid droplets; however, in the previous version of the hybrid bulk/bin microphysics scheme, solute aerosols could not nucleate ice, but an exception has now been applied to soluble organics in line with recent laboratory observations of Murray *et al.* (2010). In this version, the non-biological insoluble organics do not nucleate ice heterogeneously, because they are assumed to be highly hydrophobic.

In this model, external mixing is assumed for all solute aerosol species. Insoluble aerosols (dust, soot, insoluble organics) are assumed to be externally mixed with each other, but also internally mixed with some components of soluble aerosols and therefore able to initiate cloud droplets. The soluble fractions of the respective IN groups are shown in Table 1, following Clarke *et al.* (2004). A log-normal distribution described by Pruppacher and Klett (1997) is assumed for all aerosol size distributions with distribution parameters of each mode (geometric mean size, spectral width, ratio of total numbers between multiple modes) being constrained by observations and, in cases where observations were not available, model results from the global model for aerosol processes (GLOMAP; Spracklen *et al.*, 2005; Mann *et al.*, 2010) were used instead. These parameters are shown in Table 1 for the cases simulated in this study (TWPICE and CLASIC). In this model, insoluble aerosol particles are assumed to be aged and coated with soluble components such as sulphate on their surfaces, thus enabling them to activate both cloud droplets and cloud ice.

The semi-prognostic aerosol component treats all processes that alter aerosol loadings inside clouds (wet processes). The scheme is semi-prognostic in the sense that aerosol profiles are artificially replenished by resetting them to their initial profiles at regular time intervals of 3 h in both cases that were simulated in this study. This resetting of aerosol profiles is our numerically crude way to apply a large-scale advective forcing tendency for aerosol to compensate for aerosol loses in the domain. Depletion of aerosols occurs by in-cloud nucleation and precipitation scavenging. The aerosol mass and number mixing ratios are predicted; hence, the model is double-moment in this regard. The model tracks the mass and number mixing ratios of aerosols in the environment (i.e. those which are not activated), in clouds and in precipitation. This makes it possible for the model to account for all the sources and sinks of every aerosol particle (AP). It is not within the scope of this study to explicitly represent changes in aerosol loading due to lateral advection of aerosols into and out of the domain; hence, the population of interstitial aerosols in the air is nudged towards observed/initial profiles.

### 2.2.2. *Size distributions*

A Γ-distribution is applied to both precipitating (graupel (g), rain (r) and snow (s)) and size distributions for non-precipitating particles (cloud ice and cloud water) is according to Ferrier (1994). We use a shape parameter $\mu_r$ of 0 for rain, as in Ferrier (1994), whereas a value of $\mu_g = 2$ is used for graupel following Thompson *et al.* (2004). As for snow, a variable value of $\mu_s$ which is dependent on the mass mixing ratio $q$ is based on aircraft observations of Thompson *et al.* (2004). These predicted values of $\mu_s$ range from −2 to 3 as prescribed by Thompson *et al.* (2004). For the intercept parameters, the approach of Thompson *et al.* (2004) is applied for rain and graupel, whereas that of Heymsfield *et al.* (2002) is used the intercept parameter of snow. The slope parameters, $\lambda_x$, for all the species are chosen such that they are functions of the mass mixing ratios and are predicted using Ferrier (1994) for rain, and Thompson *et al.* (2004) for graupel and snow.

### 2.2.3. *Nucleation processes*

#### 2.2.3.1. *Initiation of cloud droplets*

The initiation of cloud droplets are treated explicitly in the model as in Phillips *et al.* (2009). All seven aerosol species described in section 2.2.1 can initiate cloud droplets. The activation of cloud particles takes place both at the cloud base and in cloud as long as the supersaturation is high enough to activate new cloud particles. At the cloud base, droplet activation from solute aerosols depends on the updraught velocity and both aerosol loading and chemistry following the Ming *et al.* (2006) scheme. In-cloud droplet formation by solute aerosols is done by the $\kappa$-Kohler theory of Petters and Kreidenweis (2007) when in-cloud supersaturations are high enough.

Insoluble aerosols are assumed to be coated by soluble materials which enable them to initiate cloud droplets. This is treated using the $\kappa$-Kohler theory of Petters and Kreidenweis (2007) at both cloud-base and in-cloud.

Table 1. Aerosol properties.

| Aerosol group | Number of modes | $\log_{10}$ of standard deviation $\log_{10}(\sigma_x)$ | Geometric mean, $Rm_x$ (μm) | Solubility parameter |
|---|---|---|---|---|
| Sulphate (SO4) | 2 | 0.30, 0.27; 0.049, 0.161 | 0.04, 0.08; 0.03, 0.18 | – |
| Sea-salt (SS) | 2; 3 | 0.30, 0.33; 0.05, 0.16, 0.26 | 0.01, 0.50; 0.03, 0.18, 4.4 | – |
| Soluble organics (SO) | 2 | 0.30, 0.27; 0.049, 0.161 | 0.04, 0.08; 0.03, 0.18 | – |
| Dust/metallic (DM) | 2 | 0.28, 0.20 | 0.8, 3.0 | 0.15 |
| Black carbon (BC) | 1 | 0.20 | 0.2 | 0.80 |
| Insoluble organics (O) | 1 | 0.20 | 0.2 | 0.80 |
| Biological aerosols (BIO) | 2 | 0.40, 0.60 | 0.17, 0.47 | 0.80 |

A comma separates the modes.
Where different aerosol specifications were applied for midlatitude continental and tropical maritime cases, a semicolon is used with the former representing CLASIC and the latter representing TWPICE.

 

*2.2.3.2. Heterogeneous nucleation of cloud ice*

As for ice nucleation, the empirical parametrization (EP) of heterogeneous ice nucleation developed by Phillips *et al.* (2008) was updated to include improvements made by Phillips *et al.* (2013). The EP model still allows nucleation from all known modes of heterogeneous ice nucleation (deposition, condensation, immersion and contact freezing) and most importantly, the scarcity of ice nucleation at subsaturated conditions and the dependence of IN on the total surface area of each aerosol species are still treated by the EP. The main property used by the EP scheme for heterogeneous ice nucleation is the baseline total surface area of all IN, whose sizes are greater than a minimum threshold of 0.1 μm. The current version of the EP has had a myriad of changes which include allowing soluble aerosols to nucleate ice crystals at very low temperatures as detailed by Phillips *et al.* (2013).

*2.2.3.3. Homogeneous freezing of cloud droplets and aerosols*

Homogeneous freezing of cloud droplets takes place at −36 °C. Preferential freezing is assumed, i.e. larger droplets freeze first depending on supersaturation and ascent velocity according to the parametrization of Phillips *et al.* (2007). Consequently, nucleation and rapid condensational growth of ice crystals ensues which leads to a reduction of supersaturation. If the water vapour dips below saturation then the smaller cloud droplets start evaporating; this can maintain the cloud close to water saturation, thus total evaporation may occur for some of the small cloud droplets without freezing. The parametrization also monitors the fraction of cloud droplets that do not freeze. Also, homogeneous freezing of interstitial aerosols is applied at low temperatures at high relative humidities near water saturation, taking into account the curvature and surface tension effects at temperatures below −40 °C.

*2.2.3.4. Ice multiplication*

Secondary multiplication of cloud ice by the Hallett–Mossop (H-M) process is modified from that of Phillips *et al.* (2009) and treated in the model at temperatures, $T$, between −3 and −8 °C by assuming that, for every milligram of liquid being accreted onto snow, PSACW or graupel, PGACW per unit time, a total of 350 small ice crystals (NIHMS and NIHMG, respectively) with initial diameters of 5 μm are ejected at −5.5 °C as:

$$NIHMS = 350\,e^6 f_{HM} T_{HM} PSACW, \quad (1)$$

$$NIHMG = 350\,e^6 f_{HM} T_{HM} PGACW, \quad (2)$$

where $f_{HM}$ is a increasing droplet size-dependent factor, which requires that no splinters be ejected by droplets of sizes less than 16 μm, and can be represented as:

$$f_{HM} = \begin{cases} 0 & \text{if } D_{CW} < 16\,\mu m, \\ 1 & \text{if } D_{CW} > 24\,\mu m, \\ \dfrac{D_{CW} - D_{min}}{D_{max} - D_{min}} & \text{elsewhere,} \end{cases}$$

where $D_{CW}$ is the cloud droplet diameter, and $D_{min}$ and $D_{max}$ are the minimum and maximum thresholds of droplet sizes for the parametrization, which are respectively 16 and 24 μm. The factor $T_{HM}$ is a triangular function of temperature which ensures that the maximum number of H-M splinters are ejected at −5.5 °C per hydrometeor:

$$T_{HM} = \begin{cases} \dfrac{8 - |T|}{2.5} & \text{if } -5.5 \geq T > -8, \\ 0 & \text{if } T \leq -8 \text{ or } T > -3, \\ \dfrac{|T| - 3}{2.5} & \text{if } -3 \geq T > -5.5. \end{cases}$$

*2.2.4. Autoconversion processes*

All the autoconversion processes, e.g. of cloud droplets to rain, cloud ice to snow and snow to graupel are being treated using a bulk parametrization approach detailed below.

Table 2. Microphysical conversion tendencies for mass mixing ratio (kg kg$^{-1}$ s$^{-1}$). The final species in each interaction is the first symbol within parentheses, while symbols after the semicolon denote the initial interacting species.

| Symbol | Meaning |
|---|---|
| $Ac(q_g; q_w \mid q_g)$ | Riming of cloud liquid by graupel |
| $Ac(q_g; q_i \mid q_g)$ | Accretion of cloud ice by graupel |
| $Ac(q_g; q_s \mid q_g)$ | Accretion of snow by graupel |
| $Ac(q_g; q_r \mid q_g)$ | Accretion of rain by graupel |
| $Ac(q_g; q_r \mid q_i)$ | Accretion of cloud ice by rain |
| $Ac(q_g/q_s; q_s \mid q_r)$ | Accr of snow by rain, to graupel or snow |
| $Ac(q_g/q_s; q_r \mid q_s)$ | Accr of rain by snow, to graupel or snow |
| $Ac(q_r; q_w \mid q_r)$ | Accretion of cloud liquid by rain |
| $Ac(q_s; q_w \mid q_s)$ | Riming of cloud liquid by snow |
| $Ac(q_s; q_i \mid q_s)$ | Accretion of cloud ice by snow |
| $Ac(q_s; q_w \mid q_i)$ | Snow from cloud ice by riming |

*2.2.4.1. Autoconversion of cloud droplets to rain*

The rate of autoconversion of rain from cloud particles, *PRAUT*, is treated using the scheme of Khairoutdinov and Kogan (2000):

$$PRAUT = 1350\, q_c^{2.47}\, n_c^{-1.79}. \quad (3)$$

This is a robust bulk parametrization based on the results of a bin-resolving model. It depends primarily on predicted cloud droplet number and mass mixing ratios $n_c$ and $q_c$, respectively.

*2.2.4.2. Autoconversion of cloud ice to snow*

The rate of conversion of cloud ice to snow follows a modified version of Ferrier (1994)'s parametrization when the slope parameter, $\lambda_i$, of the ice crystal size distribution exceeds a certain minimum threshold, $\lambda_{i0}$:

$$PSAUT = \frac{q_i}{\Delta t}\left\{1 - \left(\frac{\lambda_i}{\lambda_{i0}}\right)^3\right\}, \quad (4)$$

where $\lambda_{i0} = \Gamma(2+\mu_i)/\{150e^{-6}\Gamma(1+\mu_i)\}$ for the shape parameter, $\mu_i$ and $\Delta t$ is the model time step.

*2.2.4.3. Autoconversion of snow to graupel*

The autoconversion of snow to graupel, *PGAUT*, is dependent on the riming rate of cloud liquid onto snow. It is determined by deducting the sum of mass mixing ratios of snow gained by depositional growth, *PSDEP*, and accretion of cloud ice, *PSACI*, from the total mass gained by snow through riming, *PSACW*. Half of this difference becomes the mass of graupel gained through autoconversion (Eq. (5)). This treatment follows the semi-empirical treatment developed by Swann (1998) and requires the snow content to exceed a critical threshold of 500 μg.

$$PGAUT = 0.5(PSACW - PSDEP - PSACI). \quad (5)$$

Here, *PSDEP* is determined following the bulk parametrization of Lin *et al.* (1983). For the rates of changes of the number mixing ratios from the autoconversion processes, *NRAUT*, *NSAUT* and *NGAUT*, a critical radii of the new seeds of these species are prescribed, which are 50 μm for rain, 170 μm for snow, and finally 100 μm for graupel.

*2.2.4.4. Coagulation processes*

An emulated bin microphysics approach has been incorporated into the model for the coagulation processes shown in Table 2.

A mass grid $m_x(D_x)(j)$ of 33 sizebins is populated using Eq. (6) by prescribing a minimum diameter $D_{min,x}(j)$ at $j = 1$ for each $x$ =g, i, s, r, l and incrementing the mass from one sizebin to the next using an arbitrary multiplication factor

$$m_x(D)(1) = \frac{\pi \rho_x D_{min,x}^3}{6}, \quad (6)$$

where $\rho_x$ is the bulk density of the $x$th species.

The change in mass mixing ratio per unit time, $\Delta q_{x,y}/\Delta t$, of specie $x$ collecting specie $y$, can be computed as

$$\frac{\Delta q_{x,y}}{\Delta t} = \sum_{i=1}^{N_t}\sum_{j=1}^{N_t} \chi_{x,y}(i,j)\, n_x(i)\, n_y(j) m_y(j), \tag{7}$$

and, likewise, the change in number mixing ratio per unit time, $\Delta n_{x,y}/\Delta t$ as

$$\frac{\Delta n_{x,y}}{\Delta t} = \sum_{i=1}^{N_t}\sum_{j=1}^{N_t} \chi_{x,y}(i,j)\, n_x(i)\, n_y(j), \tag{8}$$

where $i$ and $j$ are indices of summation through the $N_t$ mass-grids, $\chi_{x,y}$ is the collection kernel for the interacting particles $x$ and $y$, $N_x$ and $M_x$ are respectively, the number and mass mixing ratios of the interacting species. These changes in mixing ratios per unit time equal the mixing ratio tendencies that are added to the evolution equations of mass and number mixing ratios at every model time step.

*2.2.4.5. Collection kernels*

The collection kernel, $\chi_{x,y}$, for the interacting particles $x$ and $y$ is proportional to the volume swept by the particles per unit time falling at relative fall velocity, $V_t = |V_{t,x,\mathrm{sfc}}(i) - V_{t,y,\mathrm{sfc}}(j)|$ and is given by:

$$\chi_{x,y}(i,j) = E_{\mathrm{c},x,y}(i,j) E_{\mathrm{s},x,y} A_{x,y}(i,j) V_t \sqrt{\frac{\rho_{\mathrm{sfc}}}{\rho_{\mathrm{a}}}}, \tag{9}$$

where $E_{\mathrm{c},x,y}$, is the collision efficiency of collisions between particles $x$ and $y$, values of which are interpolated from the Explicit Microphysics Model (EMM) results of Phillips *et al.* (2005). $E_{\mathrm{s},x,y}$ is the sticking efficiency between collisions of particles $x$ and $y$. The geometric cross-sectional area, $A_{xy}$, is given by:

$$A_{x,y}(i,j) = \pi \left\{ \frac{D_x(j)}{2} - \frac{D_y(j)}{2} \right\}^2. \tag{10}$$

$V_{t,x,\mathrm{sfc}}$ is the terminal velocity of the hydrometeor of diameter $D_{x,y}$, evaluated at the surface using an expression of the form of Eq. (11), where the coefficients are as given in Heymsfield *et al.* (2007):

$$V_t(D) = aD^b, \tag{11}$$

The last term on the right in Eq. (9), with surface air density, $\rho_{\mathrm{sfc}}$, and air density, $\rho_{\mathrm{a}}$, at a given model level is the altitude correction factor for the terminal velocity.

*2.2.4.6. Sticking efficiencies*

The sticking efficiencies, $E_{\mathrm{s},x,y}$ (Eq. (12)) for the collisions between the solid particles are computed using a new empirical parametrization developed by Phillips *et al.* (2015) using a long history of laboratory observations available in the literature. In Phillips *et al.* (2015), $E_{\mathrm{s},x,y}$ is given by

$$E_{\mathrm{s},x,y} = \exp\left\{ \frac{\beta(T) K_{\mathrm{c}}}{\alpha} \right\}, \tag{12}$$

where $\beta(T)$ is a temperature-dependent thermal smoothness coefficient that caters for the surface texture of the particles. $K_{\mathrm{c}}$ is the collision kinetic energy of the colliding particles and is proportional to the energy required to separate the particles after impact, while $\alpha$ is the surface area of the smaller particle involved in the collisions. Wet growth of graupel is also being treated in this aerosol–cloud model, hence in the case of wet growth of graupel, a sticking efficiency of unit is assumed for collisions between graupel and other solid hydrometers following Musil (1970). For collisions involving cloud liquid and rain, a sticking efficiency of unity is also imposed.

*2.2.4.7. Turbulence enhancement*

Enhancement of accretion by turbulence is also treated in this hybrid bin/bulk aerosol–cloud model. This is done by a simplified version of the turbulence enhancement scheme developed for the Hebrew University cloud model by Benmoshe and Khain (2014). The difference between our approach and that of Benmoshe and Khain (2014) is that we do not explicitly calculate the turbulent kinetic energy, which is used to determine the dissipation rate, but we empirically parametrize the dissipation rate using the data of MacPherson and Isaac (1977). The parametrization of dissipation rate, $\epsilon$, that we use is a function of vertical velocity, $w$, and is given by

$$\epsilon = 0.00954|w|. \tag{13}$$

This is the turbulence enhancement factor that is applied to all collisions in mixed-phase clouds.

*2.2.4.8. Melting*

Melting of ice is based on Eqs 16–80 of Pruppacher and Klett (2010) and, in this approach, processes for all solid hydrometeors are treated explicitly in the model. The tendencies of mass and number mixing ratios, *PXMLT* and *NXMLT* (for X = G or S or I) from the melting process are treated as sources of both number and mass mixing ratios for rain.

*2.2.4.9. Sedimentation of hydrometeors*

A bulk microphysics approach is still being used for evaluating the fall velocities of the hydrometeors following the approach of Ferrier (1994). A number-weighted fall velocity is used for the sedimentation of the number mixing ratios and a mass-weighted fall velocity is used for the fall velocity of the mass mixing ratios.

## 3. Model comparisons to observations

To ensure the model is in agreement with observations, we compare results from our model simulations to two cases of observations. We compare to ARM data from aircraft, satellite and ground-based observing platforms for the continental case (CLASIC) and the maritime case (TWPICE). The comparisons to observations were done in close collaboration with the aircraft scientists who were involved in the respective campaigns so as to interpret the observational data properly. Detailed descriptions of these campaigns are given in May *et al.* (2008), Fridlind *et al.* (2010), Allen *et al.* (2008) and Kudzotsa (2013).

### 3.1. The simulated cases

*3.1.1. The Tropical Warm Pool International Cloud Experiment (TWPICE)*

The Tropical Warm Pool International Cloud Experiment (TWPICE; May *et al.*, 2008) was a 3.5 week maritime case of deep convection. It was carried out from 17 January to 12 February 2006 over Darwin, northwestern Australia (12.425°S, 130.891°E). The campaign comprised both a dense network of ground-based, ship and air-borne observations. A fleet of four aircraft participated in the campaign flying at low and high altitude, sampling the whole column of the atmosphere up to the lower stratosphere. The campaign covered a region with a radius of about 150 km. This case is ideal for assessing our aerosol–cloud model because of the availability of spatially extensive and temporally continuous microphysical and thermodynamic data.

The flight patterns for the high-altitude flights were aimed at sampling the microphysical and aerosol properties of the cirrus clouds; hence, the flight patterns were designed to sample both the fresh anvil outflow and also the aged cirrus. As for the low-level flights, the flight patterns were designed to sample the boundary structure.

 

*3.1.1.1. Meteorological conditions*

During the active monsoon period, there was a persistence of cirrus overcast conditions over the whole domain and a prevalence of organized deep convection with cloud tops reaching as high as the tropopause, hence the fresh anvil outflow with aged cirrus (May *et al.*, 2008). The airflow during this period was westerly from the surface up to 300 hPa (Allen *et al.*, 2008). This weather pattern persisted from 17 to 22 January. From 23 January, the monsoon was suppressed and this persisted until 2 February and was characterized by a deep inland low that drove stable westerly airflow into the domain. Although a quasi-static mesoscale convective system (MCS) developed during this period, convection was suppressed and the cloud tops during this period rarely exceeded the 10 km altitude (May *et al.*, 2008; Allen *et al.*, 2008). From 3 February, an easterly airflow at 700 mb developed and was followed by three days of clear skies. In the days following the clear skies, scattered convection prevailed, which developed into a more organized multi-cellular system during the later stages of the monsoon break period (May *et al.*, 2008).

*3.1.2. The Cloud and Land Surface Interaction Campaign*

The Cloud and LAnd-Surface Interaction Campaign (CLASIC; Miller, 2007) was a three-week continental campaign studying deep convection. It was carried out from 10 to 30 June 2007 over the US Department of Energy (DOE) Atmospheric Radiation Measurement Climate Research Facility at Southern Great Plains (ARM-SGP) in Oklahoma, USA (36.61°N, 97.49°W).

*3.1.2.1. Meteorological conditions*

The campaign period for CLASIC was characterized by the wettest summer on record for Oklahoma City. It was caused by the existence of a quasi-permanent high-pressure cell that established over the southeastern USA for much of the campaign period. This high-pressure system drove low-level southeasterly airflow into Oklahoma, advecting moisture from the Gulf of Mexico. At the upper levels, a couple of slow-moving upper-level troughs coupled with this low-level pattern caused persistent convective conditions accompanied by significant amounts of rainfall during the campaign. These conditions resulted in frequent shallow convection to be the dominant process leading to clouds during the CLASIC campaign period.

*3.2. The model set-up*

In addition to general specifications of the model given in section 2.1, further conditions were applied to the model depending on the campaign being simulated. The model was initialized using domain averages of observed thermodynamic (vapour and temperature) profiles. Their corresponding thermodynamic tendencies, together with profiles of horizontal wind and pressure were used as large-scale forcing. Of this large-scale forcing, only temperature was nudged at each time step towards observed values with a relaxation time-scale of 3 h. This nudging was done only above 15 km altitude. Convection was initiated using random perturbations of moisture in the lower troposphere. It was maintained by including additional tendencies of heat and moisture due to the observed large-scale advection from a network of soundings in the simulated cases.

Aerosol profiles were prescribed for the whole model domain using aircraft observations for the simulated cases. Where observations were lacking, data were used from other similar campaigns in similar regions that were conducted concurrently with the campaign. Further details for each campaign are outlined below.

*3.2.1. The tropical maritime case – TWPICE*

A quasi-maritime and quasi-land initialization was applied to model the TWPICE case, since the campaign domain was approximately 50% over land and 50% over the ocean. A fixed sea-surface temperature of 29 °C was applied (Fridlind *et al.*, 2010; Morrison and Grabowski, 2011; Fridlind *et al.*, 2012).

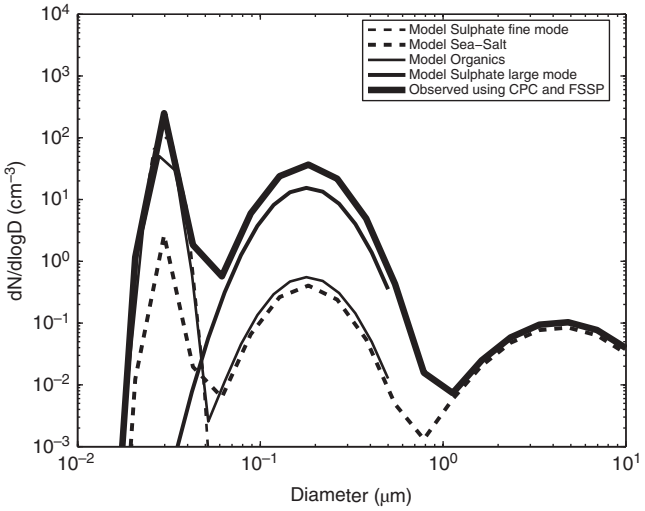


**Figure 1.** A tri-modal aerosol size distribution applied to the model for TWPICE case. Distribution parameters given by Fridlind *et al.* (2010), taken from Allen *et al.* (2008) have been applied. The species are explained in the legend.

The aerosol data in Figure 1 were derived from Allen *et al.* (2008). These data were obtained during the Aerosol and Chemical Transport In tropical conVEction (ACTIVE) campaign, a sister campaign of TWPICE studying similar convective conditions in Darwin. For the TWPICE case, there were no aerosol data obtained during the campaign and so we used aerosol data from the ACTIVE campaign instead. The campaign was conducted between November 2005 and February 2006 over Darwin, and one aircraft was deployed, the Dornier 228-101. The Dornier profiled the lower troposphere for aerosol physico-chemical properties and measured sulphate, sea-salt and organic aerosols. We assumed primary biological aerosol particles (PBAPs) to be 50% of the measured insoluble organics (Pruppacher and Klett, 1997). Black carbon (soot) and dust were not measured during the campaign; hence, we used outputs from a global tracer model, the global model of aerosol processes (GLOMAP). At higher altitudes where *in situ* measurements were not taken, the aerosols were extrapolated as homogeneously mixed and equal to the concentrations at the highest altitude taken. This is similar to the way in which other researchers (Fridlind *et al.*, 2010; Morrison and Grabowski, 2011) have treated the problem. A log-normal distribution (Figure 2) was adapted, with distribution parameters similar to those prescribed by Fridlind *et al.* (2010) in their model intercomparison study and from Matthias-Maser and Jaenicke (1995) for carbonaceous and PBAPs. The simulation was run based on the data from 0300 UTC on 17 January 2006 and ending at midnight on 12 February 2006.

*3.2.2. The midlatitude continental case – CLASIC*

As for the CLASIC case, continental specifications were imposed and a Γ-distribution was also assumed for the aerosols. The aerosol data were acquired from the Cumulus Humilis Aerosol Processing Study (CHAPS; Berg *et al.*, 2009), a sister campaign of CLASIC conducted concurrently with CLASIC. The focus of CHAPS was to obtain detailed physical, chemical and radiative properties of CCN and aerosols in general from urban pollution and contrast with their natural fields. The distribution parameters prescribed by Phillips *et al.* (2009) shown in Table 1 were used for the aerosol distribution. For aerosol profiles at altitudes above the flight ceilings, the same extrapolation technique applied for TWPICE above was also used here. The simulation was commenced at 0000 UTC on 10 June 2007 and ran to midnight 30 June 2007. For both cases, the model output was written out

 

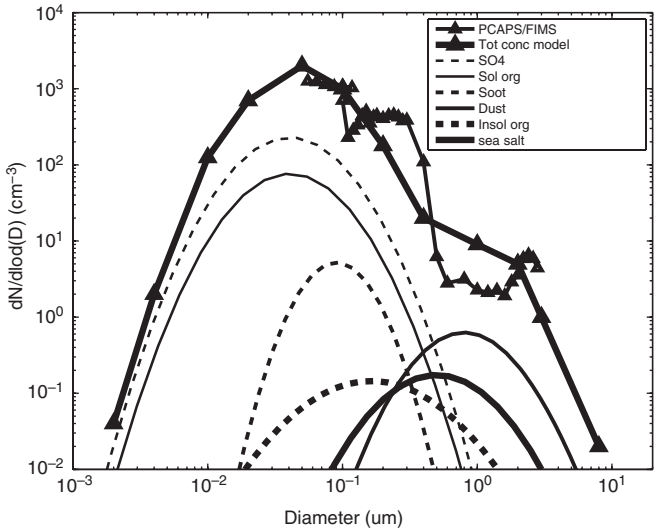


**Figure 2.** A tri-modal aerosol log-normal size distribution applied to the model for the CLASIC case. Distribution parameters prescribed by Phillips *et al.* (2009) have been applied. The respective species are as explained in the legend.

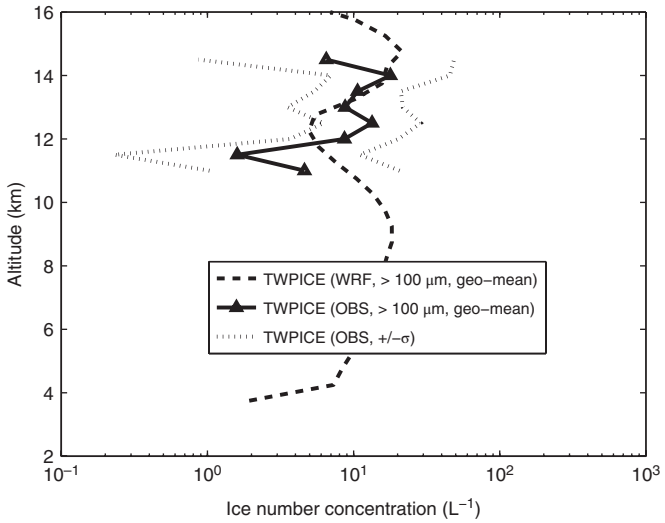


**Figure 3.** Mean number concentrations of crystals with effective diameters greater than 100 μm for TWPICE, conditionally averaged over regions of weak vertical velocities (vertical velocity less than 1 m s$^{-1}$) and cloudy regions with IWC greater than 0.001 g m$^{-3}$. The bold dashed line represents the model results, while the bold solid line is from observations. The dotted lines represent ±1 standard deviation from the mean observation line.

at 5 min intervals of the simulation time and 36 h of the model spin-up were allowed before the analysis of the model results.

## 4. Results and discussion

### *4.1. Microphysical properties*

#### *4.1.1. Ice crystal number concentrations*

In Figures 3 and 4, the vertical profiles of ice number concentration for the predicted and observed values are shown. For TWPICE, the model prediction lay within the 90% confidence interval of the population mean. This was the case for the regions where comparison with observations was possible due to the availability of observations. The bold solid curve in Figure 3 represents the observations and it represents an average of flight measurements from nine days taken during the campaign using the Cloud Imaging Probe (CIP).

The CIP (as explained above) counted all particles with diameters between 25 and 2300 μm. This size range includes giant aerosols, cloud droplets and cloud ice. We note that, at

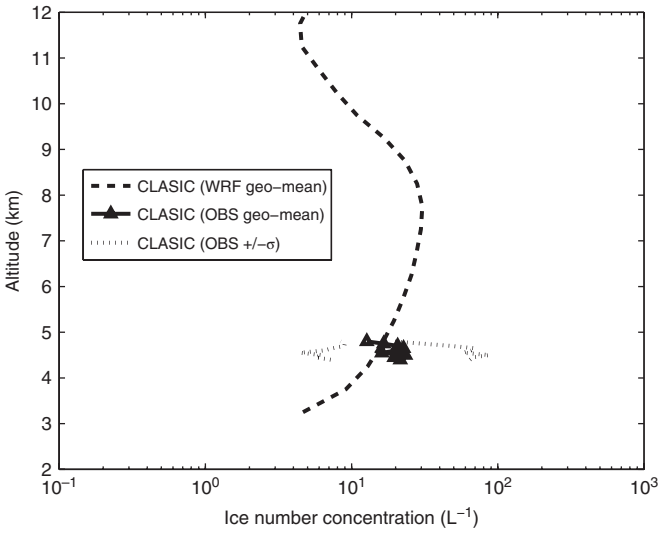


**Figure 4.** As Figure 3, but for CLASIC.

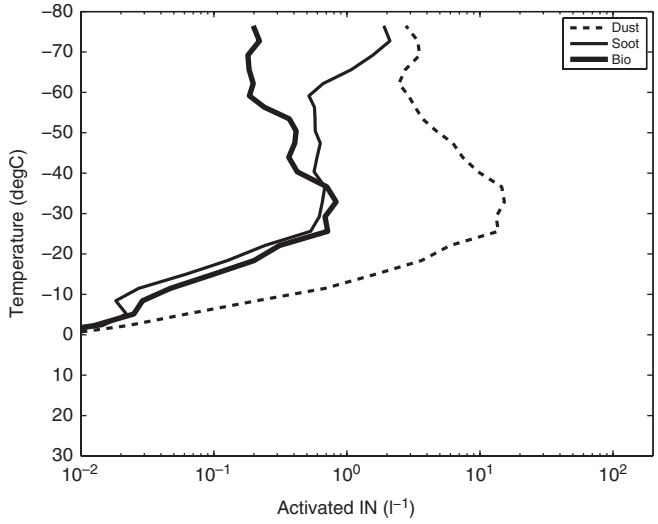


**Figure 5.** The number budgets of activated IN in TWPICE.

altitudes above the 10 km fight level, negligible amounts of giant aerosols (diameters > 25 μm) exist, owing to gravitational effects and, due to the onset of homogeneous freezing of cloud droplets at around the 9 km altitude in TWPICE, no cloud droplets would be expected in the CIP data. There is an issue of ice shattering that tends to inflate crystal number concentrations and could be acting in these observations; therefore, to address this, the CIP data were corrected for ice shattering by imposing cut-off sizes of 100 μm in the observed data. Hence, both the predicted and observed concentrations in Figure 3 are for ice crystals of sizes greater than 100 μm.

The aerosol types nucleating ice are shown as height profiles in Figures 5 and 6. They show that dust is the dominant source of heterogeneously nucleated ice crystals in the model for both TWPICE and CLASIC; however, soot and biological aerosols still have substantial contributions to the total number concentration of heterogeneously nucleated ice crystals. However it should be noted that homogeneous aerosol and cloud droplet freezing are by far the most dominant sources of ice crystals as shown in Part II of this work. The H-M process (section 2.2.3), which is an ice multiplication process, is the second most significant source of ice crystals in the model.

Observational data for ice crystal number concentrations are limited for CLASIC (Figure 4). This is because most of the flights during the campaign traversed only the lower troposphere, where water clouds were prevalent. However, we find the order of magnitude of the predicted ice number concentrations are in

 

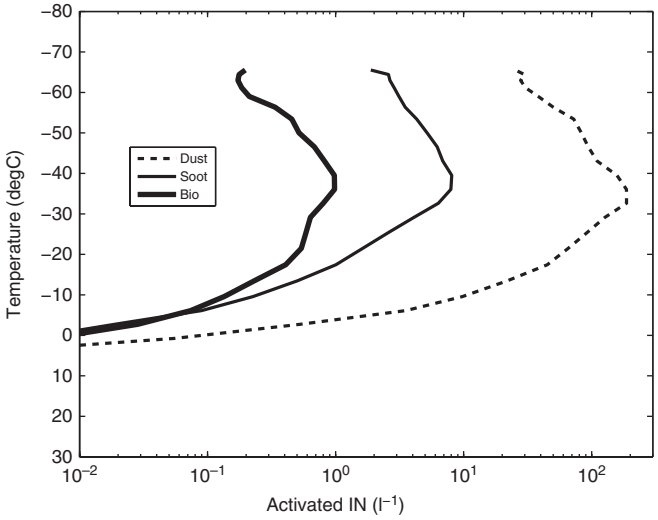


**Figure 6.** The number budgets of activated IN in CLASIC.

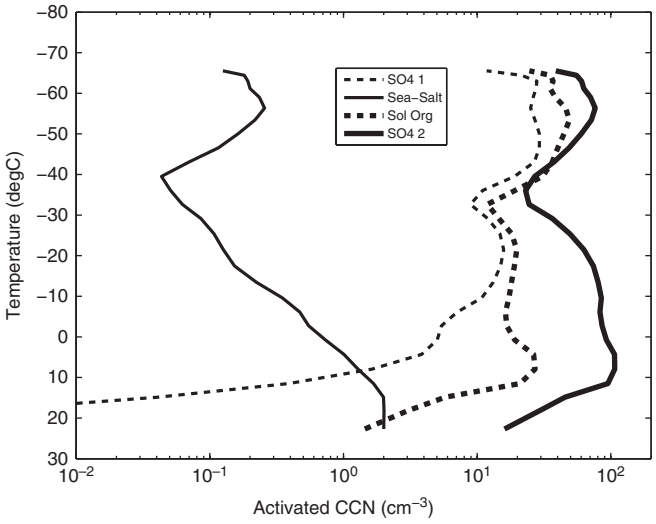


**Figure 8.** The number budgets of activated CCN in the CLASIC control run.

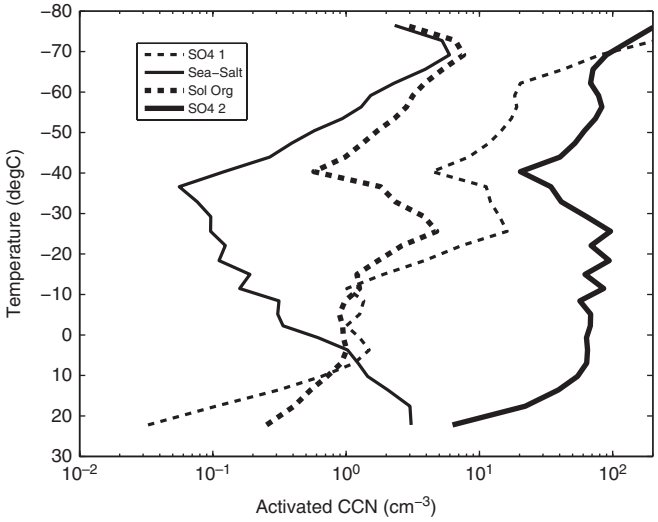


**Figure 7.** The number budgets of activated CCN in the TWPICE control run.

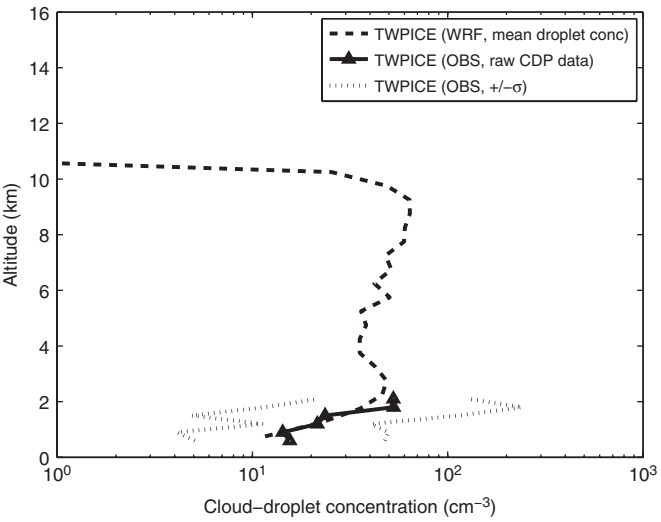


**Figure 9.** Mean number concentrations of cloud droplets for the TWPICE campaign, conditionally averaged over regions of weak vertical velocities ($<0.5\,\mathrm{m\,s^{-1}}$) and cloudy regions with ice water content $>0.001\,\mathrm{g\,m^{-3}}$. The bold lines represent the average values, while the dotted lines represent standard deviations from the mean.

good agreement with those found by other researchers (Mitchell, 1994; Kajikawa and Heymsfield, 1989) in their modelling and observational studies.

The higher ice number concentrations in CLASIC relative to TWPICE are expected for ocean and land conditions. There were higher aerosol number concentrations in the continental CLASIC than in the maritime TWPICE. The CLASIC aerosol scenario was very polluted as it was conducted near to and downwind of urban areas in Oklahoma.

A peak in ice number concentration (due to homogeneous freezing of cloud droplets and aerosols) is seen in both simulations, although it is more distinct in CLASIC than in TWPICE. This is mainly because homogeneous freezing is more favourable in continental than in maritime clouds because of the smaller cloud particles that characterize continental clouds. Smaller sizes of cloud particles delay the onset of rain, hence clouds have a higher chance of growing deeper to reach the homogeneous freezing levels.

### *4.1.2. Cloud droplet number concentrations*

By referring to both Figures 7 and 8 which show the number budgets of the sources of cloud droplets from all the different aerosol species being treated in the model, it can be seen that the accumulation mode of sulphate aerosols is the dominant source of cloud droplets, especially in TWPICE. However, in CLASIC soluble organics are equally important because of the relatively high soluble organics to sulphur ratio in CLASIC compared to TWPICE.

A Forward Scattering Spectrometer Probe (FSSP) mounted on the wing of the Dornier aircraft during the ACTIVE campaign measured droplet number concentration. The FSSP measures particles with sizes ranging from 0.5 to 32 μm and has the potential to include super-micron aerosols in its measurements of cloud droplet concentrations, hence a minimum threshold for liquid water content (LWC) of $0.001\,\mathrm{g\,m^{-3}}$ was imposed for cloud screening for FSSP data. Figures 9 and 10 show the average vertical profiles of droplet number concentrations for TWPICE and CLASIC, respectively. The observations curve in Figure 9 is an average of flight measurements taken from fourteen days of the campaign. The model results were conditionally averaged over regions of weak vertical velocities, i.e. less than $0.5\,\mathrm{m\,s^{-1}}$. This was done to match the flight patterns of the campaign; the Dornier aircraft always avoided cores of convection to avoid severe turbulence. Also, all the ACTIVE and TWPICE flights did not specifically target and sample liquid phase clouds, although there were occasional passages through shallow cumulus cloud.

For CLASIC, the Cloud, Aerosol and Precipitation Spectrometer (CAPS) probe measured the droplet number concentrations. The CAPS comprises the Cloud Aerosol Probe (CAS) and the CIP for measurements within the 0.5–50 and the 25–1550 μm

 

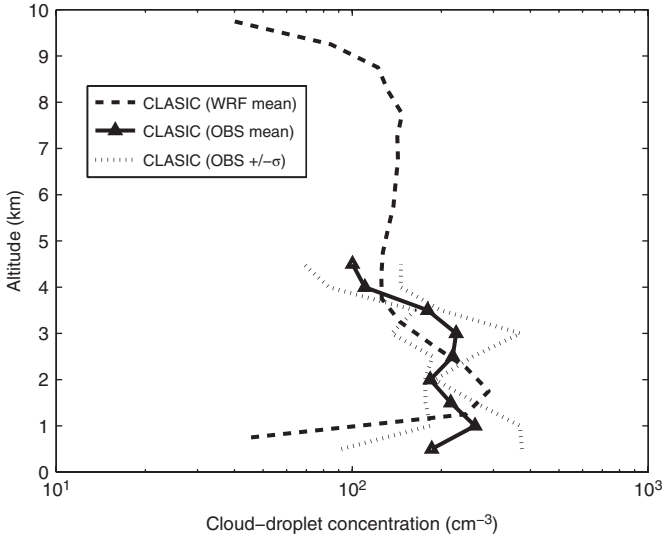


**Figure 10.** As Figure 9, but for the CLASIC campaign, conditionally averaged over regions of strong vertical velocities ($>0.5\,\mathrm{m\,s^{-1}}$) and cloudy regions with ice water content $>0.001\,\mathrm{g\,m^{-3}}$.

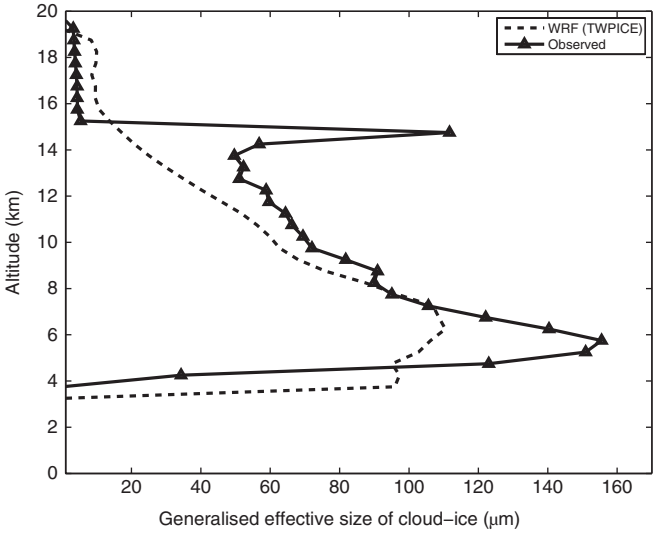


**Figure 11.** Vertical profiles of mean effective diameter of ice crystals for TWPICE, conditionally averaged over cloudy regions where effective crystal diameter was greater than zero. The bold lines represent the average values.

size ranges. The observations shown are an average of flight measurements using the CAPS probe for size bins between 5 and 50 μm (our thresholds for cloud particle sizes) taken from 13 different days of the campaign. Cloud screening was performed by selecting instances where the LWC was greater than $0.013\,\mathrm{g\,m^{-3}}$ to eliminate instances were only aerosols were detected by the CAS at its lowest sizes of the measured spectrum. CLASIC was characterized by shallow convection producing heavy precipitation, so the comparison to observations is done by conditionally averaging the predicted number concentrations of cloud droplets over clouds with vertical velocities greater than $0.5\,\mathrm{m\,s^{-1}}$.

Satisfactory agreement between observations and model results is seen in Figures 9 and 10, showing the strength of the model in resolving these microphysical processes. Also, the higher cloud droplet number concentrations in CLASIC relative to TWPICE are explicable in terms of their contrasting aerosol scenarios (as explained for ice crystal concentrations). The strong peaks in cloud droplet concentrations shown at 2 km altitude are reminiscent of the one expected at cloud bases. Since supersaturations attain their maximum values within a few metres above cloud base and decrease gently to a steady value beyond that level, so does the droplet number concentration (Rogers and Yau, 1991). The other explanation is the onset of collision and coalescence aloft, which depletes cloud number through rain production. Finally, because of preferential sedimentation of larger cloud droplets, that peak can also not be averted.

#### 4.1.3. *Mean radius of ice crystals*

The mean sizes of cloud ice are important in assessing the radiative properties of clouds, for instance in the determination of the extinction coefficient (Mitchell, 1994), which is a measure of how strongly a substance attenuates the radiative fluxes. Therefore, the model predicts the mean sizes of cloud ice and results are shown in Figure 11. A good agreement between observations and model predictions is noted for TWPICE (Figure 11). The decrease of mean crystal sizes with height is primarily due to an increase with height of the total number concentrations of ice particles (Figures 3 and 4), which increases the competition for the same amount of available vapour. Sedimentation of ice crystals out of cirrus clouds and the growth of crystals by vapour diffusion promotes riming and aggregation during descent. Other mechanisms of crystal growth such as aggregation are also effective at higher temperatures. No comparison with observations is shown for CLASIC due to the unavailability of ice-phase data; however, predictions were quite realistic for TWPICE (plot not shown).

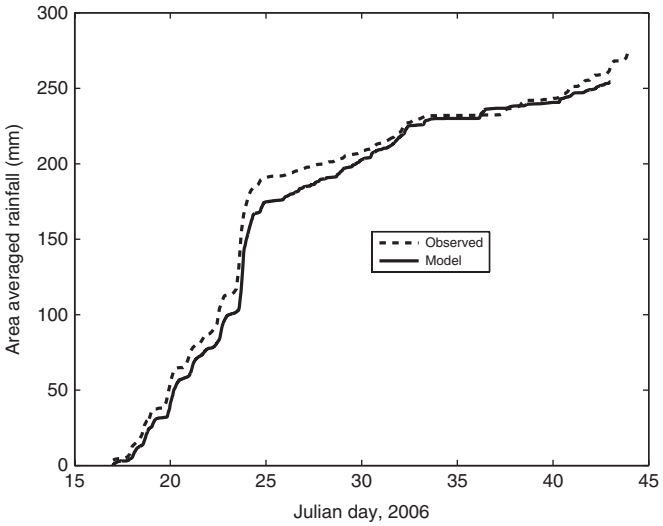


**Figure 12.** Cumulative precipitation (mm) unconditionally averaged for the whole four-week simulation period of TWPICE. The bold lines represent the average.

### 4.2. *Macrophysical properties and radiation statistics*

#### 4.2.1. *Precipitation*

Figures 12 and 13 show area-averaged cumulative precipitation that is unconditionally averaged over the whole domain of the study and over the whole simulation period for TWPICE and CLASIC, respectively. A 'near-perfect' agreement between model predictions and observations is shown in both simulations, particularly for TWPICE.

#### 4.2.2. *Radiation statistics*

Table 3 shows the radiation statistics for the upward and downward components of radiation measured at the top of the atmosphere (TOA) and at the surface for both TWPICE and CLASIC. The observations statistics were downloaded from the ARM website (http//: www.arm.gov; accessed 24 March 2016), where they are available freely for both cases.

The highest percentage bias of 33.75% for the upward component of SW radiation at TOA for TWPICE was attributed to the fact that the model predicted higher middle-level cloudiness than observations (Figure 14). This would imply a greater optical

 

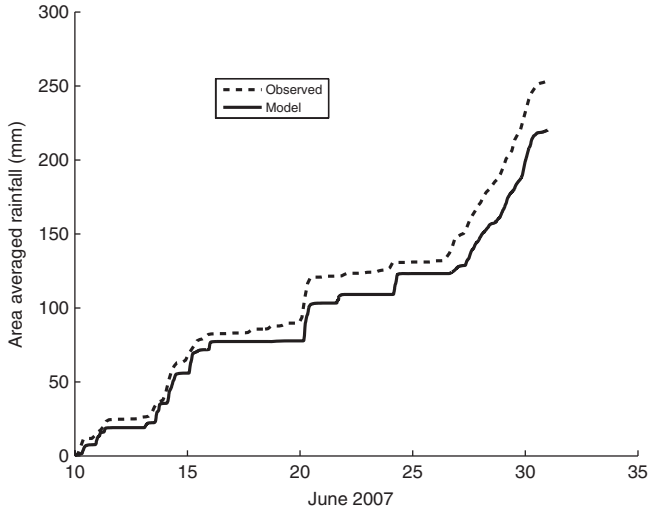


**Figure 13.** Cumulative precipitation (mm) unconditionally averaged for the whole three-week simulation period of CLASIC. The bold lines represent the average values.

Table 3. Unconditionally averaged statistics for upward and downward components of radiation for TWPICE and CLASIC.

| Radiation fluxes | Short-wave | | Long-wave | |
|---|---|---|---|---|
| ($W\,m^{-2}$) | TOA upwards | SFC downwards | TOA upwards | SFC downwards |
| Model TWPICE | 174.16 | 213.36 | 210.12 | 404.23 |
| Observed TWPICE | 130.22 | 216.06 | 201.88 | 428.16 |
| Percentage bias (%) | 33.75 | −1.25 | 4.08 | −5.56 |
| Model CLASIC | 196.69 | 240.36 | 199.89 | 371.10 |
| Observed CLASIC | 184.26 | 206.32 | 225.04 | 403.82 |
| Percentage bias (%) | 6.74 | 16.50 | −11.17 | −8.10 |

TOA = Top of the Atmosphere, SFC = Surface.

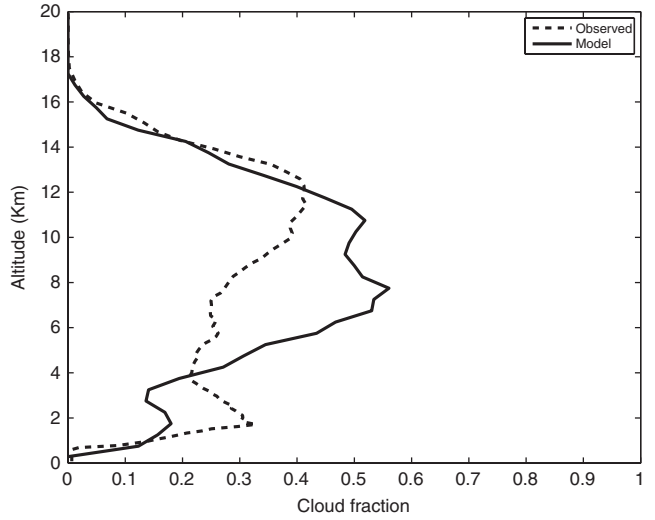


**Figure 14.** Vertical profile of cloud fraction for TWPICE averaged over the whole simulation domain for cloud mixing ratios greater than 0.01 $g\,kg^{-3}$.

depth and hence higher reflectivity in the SW range by clouds. For the same campaign, the negative bias of −5.56% in the downward component of the long-wave radiation at the surface was also attributed to the higher reflectivity of long-wave radiation in the model by clouds, since the model predicted more middle-level clouds. This negative bias was also augmented by the strong temperature dependence of the emitted radiative flux (Stefan–Boltzmann law). Figures 15 and 16 show that the model is generally colder than observations, implying that the predicted clouds would also be colder than observations, and hence the

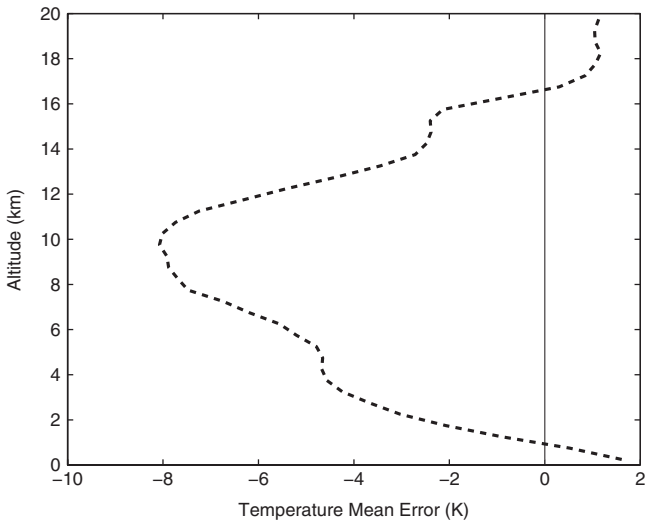


**Figure 15.** Unconditionally averaged vertical profile of temperature bias (model mean minus observations mean) for TWPICE.

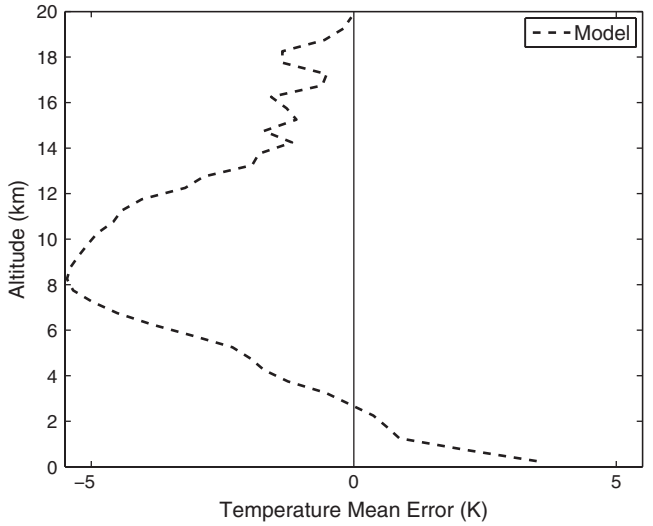


**Figure 16.** Unconditionally averaged vertical profile of temperature bias (model mean minus observations mean) for CLASIC.

long-wave radiation emitted downwards by the predicted clouds would be lower than observed.

For CLASIC, it is not immediately explicable from the available analysis why a higher positive bias of 17% is available for the downward component of short-wave radiation at the surface, but meagre evidence available in Figure 17 suggests that, on average, the model predicted slightly less cloudiness than observations, and thus more insolation was transmitted to the surface and the model systematically predicted less LWC than observations; hence the optical thickness of clouds predicted in the model was less than that of observed clouds. All other biases are within an acceptable absolute deviation from observed values of less than ±10%. This satisfactory model performance for the radiation statistics is crucial for the core objective of this study, which is the investigation of aerosol–cloud interactions. Accurate assessment and quantification of the optical properties of clouds require high confidence in the prediction of radiative fluxes, both at the top of the atmosphere and at the surface.

## 5. Conclusions

A series of model developments were carried out in this study as elaborated in section 2. Subsequently, the comparison of the model results with observations were performed by simulating two contrasting tropical scenarios of deep convection, the Tropical

 

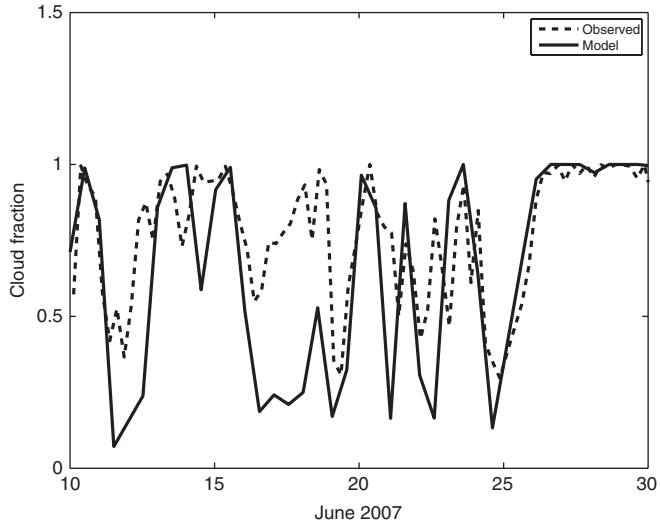


**Figure 17.** Time series of cloud fraction for CLASIC averaged over the whole simulation domain for cloud mixing ratios greater than 0.01 g kg$^{-3}$.

Warm Pool-International Cloud Experiments (TWPICE) and Cloud and LAnd Surface Interactions Campaign (CLASIC), which are respectively maritime and continental. Some of the fields compared with observations have been presented in the results sections. Where comparison was possible, the comparison of the model results to observations has shown satisfactory agreement between model simulations and observations, with the model standard deviations being within a reasonable range of less than 40% of the model mean values. The available observation dataset was obtained from a dense network of ground-based observation platforms, aircraft, ships and satellites.

Predictions of both crystal and droplet number concentrations lie within the 90% confidence intervals of observations. Similar proximity of predictions to observed scenarios was also noted for mean sizes of ice crystals. These microphysical properties are of great importance in radiation and aerosol–cloud interactions for determining the optical properties of clouds. Precipitation has also been predicted more accurately by the scheme for both cases, and especially for CLASIC. This further affirms the robustness of the model. Moreover, the radiation statistics were also simulated satisfactorily, with a model bias of less than $\pm$25% for both TOA and surface radiative fluxes. Downward and upward components of long- and short-wave radiations were predicted for both cases.

This scheme has been improved and upgraded, making it adaptable to a wide range of atmospheric science studies, particularly investigations of aerosol–cloud interactions. This updated and rigorously validated aerosol–cloud model allows research of aerosol indirect effects and was used to investigate the different mechanisms of aerosol indirect effects particularly on glaciated clouds. This study was the first of its kind using such a robust, state-of-the-art microphysics scheme comprising a semi-prognostic aerosol component, encapsulating diverse aerosol species and explicitly treating their loadings and chemical compositions. The focus of Part II of this study is to investigate different and salient mechanisms by which changes in aerosol fields, both in their number concentration and chemical composition, affect the optical properties of clouds. The main objectives of the study will be to explore the cloud microphysical and dynamical mechanisms for glaciated cloud indirect effects on the mesoscale, focusing mainly on glaciation, thermodynamic and riming indirect effects (Lohmann and Feichter, 2005) from anthropogenic soluble and solid aerosols. Important feedbacks associated with these indirect effects are investigated, as well as quantifying their respective radiative forcings. This will done by way of sensitivity tests.

## Acknowledgements

The work was funded by an award to, and was directed by, Vaughan T. J. Phillips (VTJP) from the Office of Science (BER), US Department of Energy (DE-SC0002383, which later became DE-SC0007396). The authors are also grateful to the anonymous reviewers for their constructive criticism.

## References

Allen G, Vaughan G, Bower KN, Williams PI, Crosier J, Flynn M, Connolly P, Hamilton JF, Lee JD, Saxton JE, Watson NM, Gallagher M, Coe H, Allan J, Choularton TW, Lewis AC. 2008. Aerosol and trace-gas measurements in the Darwin area during the wet season. *J. Geophys. Res: Atmos.* **113**: D06306, doi: 10.1029/2007JD008706.

Benmoshe N, Khain A. 2014. The effects of turbulence on the microphysics of mixed-phase deep convective clouds investigated with a 2D cloud model with spectral bin microphysics. *J. Geophys. Res: Atmos.* **119**: 207–221, doi: 10.1002/2013JD020118.

Berg LK, Berkowitz CM, Ogren JA, Hostetler CA, Ferrare RA, Dubey MK, Andrews E, Coulter RL, Hair JW, Hubbe JM, Lee Y-N, Mazzoleni C, Olfert J, Springston SR. 2009. Overview of the cumulus humilis aerosol processing study. *Bull. Am. Meteorol. Soc.* **90**: 1653–1667, doi: 10.1175/2009BAMS2760.1.

Boucher O, Randall D, Artaxo P, Bretherton C, Feingold G, Forster P, Kerminen V-M, Kondo Y, Liao H, Lohmann U, Rasch P, Satheesh SK, Sherwood S, Stevens B, Zhang XY. 2013. *Clouds and Aerosols in Climate Change 2013: The Physical Science Basis. Contribution of Working Group I to the Fifth Assessment Report of the Intergovernmental Panel on Climate Change*. Cambridge University Press: Cambridge, UK and New York, NY.

Charlson R, Schwartz SE, Hales J, Cess R, Coakley JA, Hansen JE, Hofmann DJ. 1992. Climate forcing by anthropogenic aerosols. *Science* **255**: 423–430.

Clark TL. 1974. A study of cloud phase parameterization using the gamma distribution. *J. Atmos. Sci.* **31**: 142–155.

Clarke AD, Shinozuka Y, Kapustin VN, Howell S, Huebert B, Doherty S, Anderson T, Covert D, Anderson J, Hua X, Moore KG, McNaughton C, Carmichael G, Weber R. 2004. Size distributions and mixtures of dust and black carbon aerosol in Asian outflow: Physiochemistry and optical properties. *J. Geophys. Res: Atmos.* **109**: D15S09, doi: 10.1029/2003JD004378.

Ferrier SB. 1994. A double-moment multiple-phase four-class bulk ice scheme. Part I: Description. *J. Atmos. Sci.* **51**: 249–280.

Fridlind AM, Ackerman A, Petch JC, Field p, Hill AA, McFarquhar G, Xie S, Zhang M. 2010. 'ARM/GCSS/SPARC TWP-ICE CRM intercomparison study', Technical report NASA-TM-2010-215858, Rept-201003234. NASA Goddard: New York, NY.

Fridlind AM, Ackerman AS, Chaboureau J-P, Fan J, Grabowski WW, Hill A, Jones TR, Khaiyer MM, Liu G, Minnis P, Morrison H, Nguyen L, Park S, Petch JC, Pinty J-P, Schumacher C, Shipway B, Varble AC, Wu X, Xie S, Zhang M. 2012. A comparison of TWP-ICE observational data with cloud-resolving model results. *J. Geophys. Res.* **117**: D05204, doi: 10.1029/2011JD016595.

Gettelman A, Liu X, Barahona D, Lohmann D, Chen C. 2012. Climate impacts of ice nucleation. *J. Geophys. Res: Atmos.* **117**: D20201, doi: 10.1029/2012JD017950.

Haywood J, Boucher O. 2000. Estimates of the direct and indirect radiative forcing due to tropospheric aerosols: A review. *Rev. Geophys.* **38**: 513–543.

Heymsfield A, Bansemer A, Field P, Durden S, Stith J, Dye J, Hall W, Grainger C. 2002. Observations and parameterizations of particle size distributions in deep tropical cirrus and stratiform precipitating clouds: Results from *in situ* observations in TRMM field campaigns. *J. Atmos. Sci.* **59**: 3457–3491.

Heymsfield A, Bansemer A, Twohy C. 2007. Refinements to ice particle mass dimensional and terminal velocity relationships for ice clouds: Part 1: Temperature dependence. *J. Atmos. Sci.* **64**: 1047–1067, doi: 10.1175/JAS3890.1.

Hill AA, Dobbie S. 2008. The impact of aerosols on non-precipitating marine stratocumulus. II: The semi-direct effect. *Q. J. R. Meteorol. Soc.* **134**: 1155–1165, doi: 10.1002/qj.277.

Johnson BT. 2003. 'The semi-direct aerosol effect', PhD thesis. University of Reading, UK.

Johnson BT, Shine K, Forster P. 2004. The semi-direct aerosol effect: Impact of absorbing aerosols on marine stratocumulus. *Q. J. R. Meteorol. Soc.* **130**: 1407–1422.

Kajikawa M, Heymsfield AJ. 1989. Aggregation of ice crystals in cirrus. *J. Atmos. Sci.* **46**: 3108–3121, doi: 10.1175/1520-0469(1989)046<3108:AOICIC>2.0.CO;2.

Kessler E. 1969. On the distribution and continuity of water substance in atmospheric circulations. *Meteorol. Monogr.* **10**: 82–84.

Khairoutdinov M, Kogan Y. 2000. A new cloud physics parameterization in a large-eddy simulation model of marine stratocumulus. *Mon. Weather Rev.* **128**: 229–243.

Koch D, Genio AD. 2010. Black carbon semi-direct effects on cloud cover: Review and synthesis. *Atmos. Chem. Phys.* **10**: 7685–7696.

 

Kudzotsa I. 2013. 'Mechanisms of aerosol indirect effects on glaciated clouds simulated numerically', PhD thesis. University of Leeds, UK.

Liao H, Seinfeld JH. 1998. Effect of clouds on direct aerosol radiative forcing of climate. *J. Geophys. Res: Atmos.* **103**: 3781–3788, doi:10.1029/97JD03455.

Lim KSS, Hong YS. 2010. Development of an effective double-moment cloud microphysics scheme with prognostic cloud condensation nuclei (CCN) for weather and climate models. *Mon. Weather Rev.* **138**: 1587–1612, doi: 10.1175/2009MWR2968.1.

Lin YL, Farley RD, Orville HD. 1983. Bulk parameterization of the snow field in a cloud model. *J. Clim. Appl. Meteorol.* **22**: 1065–1092.

Lohmann U, Feichter J. 2001. Can the direct and semi-direct aerosol effect compete with the indirect effect on a global scale? *Geophys. Res. Lett.* **28**: 159–161, doi: 10.1029/2000GL012051.

Lohmann U, Feichter J. 2005. Global indirect aerosol effects: A review. *Atmos. Chem. Phys.* **5**: 715–737, doi: 10.5194/acp-5-715-2005.

Lohmann U, Stier P, Hoose C, Ferrachat S, Kloster S, Roeckner E, Zhang J. 2007. Cloud microphysics and aerosol indirect effects in the global climate model ECHAM5-HAM. *Atmos. Chem. Phys.* **7**: 3425–3446.

McComiskey A, Feingold G. 2012. The scale problem in quantifying aerosol indirect effects. *Atmos. Chem. Phys.* **12**: 1031–1049.

MacPherson J, Isaac G. 1977. Turbulent characteristics of some Canadian cumulus clouds. *J. Appl. Meteorol.* **16**: 81–90.

Mann G, Carslaw K, Spracklen D, Ridley D, Manktelow P, Chipperfield M, Pickering S, Johnson C. 2010. Description and evaluation of GLOMAP-mode: A modal global aerosol microphysics model for the UKCA composition-climate model. *Geosci. Model Dev.* **3**: 519–551.

Matthias-Maser S, Jaenicke R. 1995. The size distribution of primary biological aerosol particles with radii $> 0.2\,\mu$m in an urban/rural influenced region. *Atmos. Res.* **39**: 279–286.

May PT, Mather JH, Vaughan G, Bower KN, Jakob C, McFarquhar GM, Mace GG. 2008. The tropical warm pool international cloud experiment. *Bull. Am. Meteorol. Soc.* **89**: 629–645, doi: 10.1175/BAMS-89-5-629.

Menon S, Genio AD, Del Koch D, Tselioudis G. 2002a. GCM simulations of the aerosol indirect effect: Sensitivity to cloud parameterization and aerosol burden. *J. Atmos. Sci.* **59**: 692–713, doi: 10.1175/1520-0469(2002)059-0692:GSOTA-2.0.CO;2.

Miller MA. 2007. 'SGP cloud and land surface interaction campaign (clasic): Science and implementation plan'. Report DOE/SC-ARM-0703. US Department of Energy. https://www.arm.gov/publications/program (accessed 26 March 2016).

Ming Y, Ramaswamy V, Donner LJ, Phillips VTJ. 2006. A new parameterization of cloud droplet activation applicable to general circulation models. *J. Atmos. Sci.* **63**: 1348–1356.

Mitchell DL. 1994. A model predicting the evolution of ice particle size spectra and radiative properties of cirrus clouds. Part I: Microphysics. *J. Atmos. Sci.* **51**: 797–816.

Mitchell DL, Arnott WP. 1994. A model predicting the evolution of ice particle size spectra and radiative properties of cirrus clouds. Part II: Dependence of absorption and extinction on ice crystal morphology. *J. Atmos. Sci.* **51**: 817–832.

Morrison H, Grabowski WW. 2011. Cloud-system resolving model simulations of aerosol indirect effects on tropical deep convection and its thermodynamic environment. *Atmos. Chem. Phys.* **11**: 10503–10523, doi: 10.5194/1cp-11-10503-2011.

Murray BJ, et al. 2010. Heterogeneous nucleation of ice particles on glassy aerosols under cirrus conditions. *Nat. Geosci.* **3**: 233–237, doi: 10.1038/ngeo817.

Musil DJ. 1970. Computer modeling of hailstone growth in feeder clouds. *J. Atmos. Sci.* **27**: 474–482.

Myhre G et al. 2009. Modelled radiative forcing of the direct aerosol effect with multi-observation evaluation. *Atmos. Chem. Phys.* **9**: 1365–1392.

O'Donnell D, Tsigaridis K, Feichter J. 2011. Estimating the direct and indirect effects of secondary organic aerosols using ECHAM5-HAM. *Atmos. Chem. Phys.* **11**: 8635–8659.

Petters MD, Kreidenweis SM. 2007. A single parameter representation of hygroscopic growth and cloud condensation nucleus activity. *Atmos. Chem. Phys.* **7**: 1961–1971, doi: 10.5194/acp-7-1961-2007.

Phillips VTJ, Andronache C, Sherwood SC, Bansemer A, Conant WC, DeMott PJ, Flagan RC, Heymsfield A, Jonsson H, Poellot M, Rissman TA, Seinfeld JH, Vanreken T, Varutbangkul V, Wilson JC. 2005. Anvil glaciation in a deep cumulus updraught over Florida simulated with the explicit microphysics model. I: Impact of various nucleation processes. *Q. J. R. Meteorol. Soc.* **131**: 2019–2046, doi: 10.1256/qj.04.85.

Phillips VTJ, Donner LJ, Garner ST. 2007. Nucleation processes in deep convection simulated by a cloud-system-resolving model with double-moment bulk microphysics. *J. Atmos. Sci.* **64**: 738–761, doi: 10.1175/JAS3869.1.

Phillips VTJ, DeMott PJ, Andronache C. 2008. An empirical parameterization of heterogeneous ice nucleation for multiple chemical species of aerosol. *J. Atmos. Sci.* **65**: 2757–2783, doi: 10.1175/2007JAS2546.1.

Phillips VTJ, Andronache C, Morris BCE, Sands DC, Bansemer A, Lauer A, McNaughton C, Seman C. 2009. Potential impacts from biological aerosols on ensembles of continental clouds simulated numerically. *Biogeosciences* **6**: 987–1014.

Phillips VTJ, DeMott PJ, Andronache C, Pratti KA, Twohy C. 2013. Improvements to an empirical parameterization of heterogeneous ice nucleation and its comparison with observations. *J. Atmos. Sci.* **70**: 378–409.

Phillips VTJ, Formenton M, Bansemer A, Kudzotsa I, Lienert B. 2015. A parameterization of sticking efficiency for collisions of snow and graupel with ice crystals: Theory and comparison with observations. *J. Atmos. Sci.* **72**: 4885–4902.

Pruppacher HR, Klett JD. 1997. *Microphysics of Clouds and Precipitation*. Kluwer Academic/Springer: Berlin.

Pruppacher HR, Klett JD. 2010. *Microphysics of Clouds and Precipitation*, Vol. 18. Reidel/Springer: Berlin.

Reisner J, Rasmussen RM, Bruintjes RT. 1998. Explicit forecasting of supercooled liquid water in winter storms using the MM5 mesoscale model. *Q. J. R. Meteorol. Soc.* **124**: 1071–1107.

Rogers RR, Yau MK. 1991. *A Short Course in Cloud Physics* (3rd edn). Pergamon/Elsevier: Oxford, UK.

Solomon S, Qin D, Manning M, Chen Z, Marquis M, Averyt K, Tignor M, Miller HL. (eds.) 2007. *Climate Change 2007: The Physical Science Basis. Contribution of Working Group I to the Fourth Assessment Report of the Intergovernmental Panel on Climate Change*. Cambridge University Press: Cambridge, UK and New York, NY.

Spracklen D, Pringle K, Carslaw K, Chipperfield M, Mann G. 2005. A global off-line model of size-resolved aerosol microphysics: I. Model development and prediction of aerosol properties. *Atmos. Chem. Phys.* **5**: 2227–2252, doi: 10.5194/acp-5-2227-2005.

Thompson G, Rasmussen RM, Manning K. 2004. Explicit forecasts of winter precipitation using an improved bulk microphysics scheme. Part I: Description and sensitivity analysis. *Mon. Weather Rev.* **132**: 519–542.

Walko RL, Cotton WR, Meyers MP, Harrington JY. 1995. New RAMS cloud microphysics parameterization. Part I: The single-moment scheme. *Atmos. Res.* **38**: 29–62.

 